Applying Neural Network Model for Adsorption Methyl Paraben (MP) Dye Using *Ricinus Communis*-capeed Fe_3O_4 NPs Synthesized from Aqueous Solution

Marahel, Farzaneh*+; Mombeeni Goodajdar, Bijan; Basari, Neda; Niknam, Leila; Ghazali, Amir Abbas

Department of Chemistry, Omidiyeh Branch, Islamic Azad University, Omidiyeh, I.R. IRAN

ABSTRACT: *The applicability of the synthesized Ricinus Communis-capeed Fe_3O_4NPs as a novel adsorbent for eliminating Methyl Paraben (MP) from aqueous media was investigated. Various techniques including Brunauer Emmett Teller theory (BET), Fourier Transform InfraRed (FT-IR) spectroscopy, X-Ray Diffraction (XRD), Scanning Electron Microscopy (SEM), and Energy Dispersive X-ray (EDX) were used to characterize this novel adsorbent. The maximum adsorption efficiency of (MP) dye onto Ricinus Communis-capeed Fe_3O_4 NPs was 98.6% at an optimum pH value of 7.0, the adsorbent dosage of 0.01 g, (MP) dye concentration of 15 mg/L, and contact time of 12 min were considered as the ideal values for (MP) dye. The adsorption data fitted well with the Langmuir isotherm model with a correlation coefficient ($R^2 > 0.97$), whereas the adsorption kinetics followed the pseudo-second-order kinetics. The use of an artificial neural network model in predicting data with the Levenberg–Marquardt algorithm, purlin, or a linear transfer function at the output layer, and training was helpful. ANN model as a tool (mean square error) MSE_{ANN} = 0.0034, MSE_{FL} = 0.023, and MSE_{ANFIS} = 0.0020 for removal of the MP dye onto Ricinus Communis-capeed Fe_3O_4 NPs synthesis. Thermodynamic parameters of free energy (ΔG^0), enthalpy (ΔH^0), and entropy (ΔS^0) of adsorption were determined using isotherms. ΔH^0=59.58 kJ/mol, ΔG^0= -2.8324 kJ/mol and ΔS^0=221.15 kJ/mol. K. The value of (ΔG^o, ΔH^o, and ΔS^o) confirmed the sorption process was endothermic reflecting the affinity of Ricinus Communis-capeed Fe_3O_4NPs for removing MP dye onto Ricinus Communis-capeed Fe_3O_4NPs process requires heat. The maximum monolayer capacity (q_{max}) was observed to be 195.0 mg/g for MP dye at desired conditions.*

KEYWORDS: *Adsorption capacity; Methyl Paraben (MP); Neural network model; Kinetic; Thermodynamic.*

INTRODUCTION

The severity of water pollution has resulted from the economic development adopted by humans overall the world. Textile industries consume huge quantities of water and generate an enormous amount of impurities including dyes, detergents, additives, suspended solids, aldehydes, heavy metals, non-biodegradable matter, and insoluble

***** *To whom correspondence should be addressed.*
+ *E-mail: Farzane.marahel.fm@gmail.com*
1021-9986/2022/7/2358-2377 20/$/7.0

substances [1]. According to recent reports, more than one million dyes are commercially available with an annual production of over 7×10^5 tons. The textile industry worldwide consumes approximately1×10^4 tons of dyes annually and discharges nearly 100 tons/year of dyes into wastewater [1,2]. Wastewaters in industries like textile, paper, rubber, plastic, leather, cosmetic, food, and drug industries contain dyes and pigments which are hazardous and can cause allergic dermatitis, skin irritation, cancer, and mutation in living organisms [3]. Also, inhalation of them can affect the respiratory tract with symptoms of rapid or difficult breathing, while mouthing ingestion can affect the gastrointestinal tract with symptoms of burning sensation, nausea, vomiting, hyperhidrosis disorder, cognitive impairment disorder, micturition disorder, and methemoglobinemia–like syndromes [4].

Parabens as a series of p-hydroxybenzoate acids are synthetic chemicals utilized as preservatives and antimicrobials in various products, especially Personal Care Products (PCPs), pharmaceuticals, food, beverages, and industrial [5,6]. The four widely used preservatives in daily-use products include methylparaben (MP), ethylparaben (EP), propylparaben (PP), and butylparaben (BP), which are either used singly or in combination [7,8]. Some published studies have also reported that concentrations of parabens are able to cause male reproductive disorders. Due to all the above applications of parabens, they are routed to wastewater treatment plants. Parabens are removed to a considerable extent in some wastewater treatment technologies. Nevertheless, they have been identified in river water samples at the low mg/L level. Moreover, parabens have been detected in soil and sediment samples [9-11]. Therefore, it is necessary to remove toxic dyes from industrial wastewater before discharging.

The adsorption method is especially suitable for solving dyes, environmental, gases, and metals problems and has many advantages, so it has become the focus and hot spot of research. In comparison with other conventional techniques (ion exchange, biological treatments, and electrolysis), adsorption is one of the most successful and uncomplicated techniques for the deletion of toxic and noxious contaminations. Its popularity is due to advantages including higher efficiency lower waste, and facile and mild operational conditions. The successfulness of adsorption techniques in the deletion of pollutants especially those which are extremely stable in the biological degradation process *via* economically accomplishable mild ways [12-14]. Thus, the extensive utilization of adsorption techniques for the deletion of numerous chemicals from aqueous solutions seems logical [15,16]. In recent years, it was tried to eliminate specified organics from water samples by applying diverse potential adsorbents. In this connection, Magnetic NanoParticles (MNPs) as unique adsorbents thanks to their small diffusion resistance, high adsorption capacity, and large surface area have extensively been noticed. Their application for instance, in the separation of chemical species like dyes, environmental pollutants, gases, and metals has proven to be successful [17,18]. Iron oxide nanoparticles are widely used for metal remediation due to their low toxicity and easy separation from water media in addition, where the NanoParticle (NP) is composed of magnetite, a facile magnetic separation of NPs, along with associated contaminants, can be performed. However, bare magnetite nanoparticles rapidly aggregate in aqueous systems and are highly susceptibleto transformations under many environmental conditions [19,20].

This study, was to evaluate the use of an artificial neural network (ANN) model to predict the MP dye removal by *Ricinus Communis*-capeed Fe_3O_4 NPs. ANN is a numerical estimation technique, which is used to find nonlinear relationships between input and output variables. Neural networks were used been widely applied in a variety of topics such as the modeling of wastewater and aqueous solutions. Treatment and biodegradation procedures not only are based on expensive and complex processes but also produce noxious by-products. On the other hand elimination of MP dye based on biological treatment precipitation has low efficiency and is not environmentally friendly. Therefore, preparing *Ricinus Communis*-capeed Fe_3O_4 NPs as an alternative to exorbitant or noxious adsorbents for the elimination of MP dye from wastewater attracted our attention. In the process of MP dye deletion, shown structured MP dye in Fig. 1, the effects of important variables like contact time, pH of the solution, adsorbent dosage, and MP dye concentration as well as the dye deletion percentage as a response were investigated and optimized. The fact that the pseudo-second-order rate equation matched the adsorption of MP dye was evident. Also, the Langmuir model could get better than other models in explaining the equilibrium data.

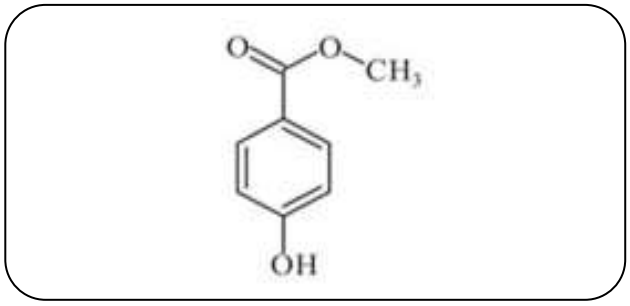

Fig. 1: The structures of Methyl Paraben (MP).

However specific isotherm models viz, Freundlich, Langmuir, Dubinin–Radushkevich, and Temkin were used to fit the experimental equilibrium data. But eventually, the findings confirmed the suitability and applicability of the Langmuir model. Moreover, it was shown that the kinetic of the adsorption process between the kinetic models of pseudo-first-order and pseudo-second-order diffusion models were under the control of the latter one. The capability of *Ricinus Communis*-capeed Fe_3O_4NPs in eliminating MP dye from aqueous solutions was demonstrated by the evidence.

EXPERIMENTAL SECTION

Material and methods

Methyl Paraben (MP) dye (99.0%) was purchased from (Razi Chemistry. Iran), and the stock solution (100 mg/L) of MP was prepared by dissolving 10 mg of MP in 100 mL distilled water. Iron(III) Chloride Hexahydrate (99.0%), and Iron(II) Chloride tetrahydrate (98.0%). Sodium hydroxide (98.0%), hydrochloric acid (37.0%), and nitric acid (69.0%). They were supplied by Merck (Darmstadt, Germany). All used chemicals were of reagent grade and utilized without further purification. For the pH adjustment, hydrochloric acid (HCl_{aq}) and sodium hydroxide ($NaOH_{aq}$) were applied.

Reagents and instruments

UV–vis spectrophotometer (Jasco, Model UV–Vis V-530, Japan). Fourier Transform InfraRed (FT-IR) spectra were recorded on a Perkin Elmer (FT-IR spectrum BX, Germany). The morphology of samples was studied by Scanning Electron Microscopy (SEM: KYKY-EM 3200, Hitachi Company, China) under an acceleration voltage of 26kV). The pH/Ion meter (model-728, Metrohm Company, Switzerland, Swiss) was used for the pH measurements. Laboratory glassware was kept overnight in 10% nitric acid solution.

The following steps show the preparation of *Ricinus Communis*: first, the leaves of the *Ricinus Communis* were picked. Second, they were washed completely with plenty of water and dishwashing liquid. Then at ambient temperature, first they were hung out to dry and then were dried at 80°C. The carbon was dissolved by grinding and milling the carbon black, for separating and grinding with a mesh of 80-100 or 100-200. Micro-leaf particles were put in a solution of chloride and concentrated nitric acid for 12 hours. Next, the carbon was cleaned and washed twice with DW (distilled water) till the pH of the water below the filter became approximately 7. The carbons were desiccated in an oven for 24 hours at a temperature of about 100°C and poured into a plastic container in an anti-moisture container [21].

Preparation Ricinus Communis-capeed Fe_3O_4 NPs

Fe_3O_4NPs were prepared by mixing $FeCl_2{\cdot}4H_2O$ (2.74 g), $FeCl_3{\cdot}6H_2O$ (3.11 g) and 0.85 mL concentrated hydrochloric acid into 25 mL deionized water. The mixture was added to a stirred 250 mL NaOH solution (1.5 M). In the designed method, the synthesis of Fe_3O_4NPs was done by introducing nitrogen gas through a sparer into the solution for oxygen removal. The bubbling of nitrogen gas through the solution protects Fe_3O_4 against critical oxidation and reduces the particle size when compared to synthesis methods without oxygen removal [22].

During the whole process, the solution temperature was maintained at 80°C. After completion of the reaction, the obtained Fe_3O_4NPs were separated from the reaction medium by the magnetic field, then we increased the bath temperature to 90°C. The sediment suspension was stirred for 3 hours. Stirring was stopped and the suspension was placed in the laboratory for 2 hours. The carbon-produced suspensions were prepared from a leaf medlar with an equal weight ratio and after analysis, BET, XRD, FT-IR, and SEM were used as adsorbents.

Batch adsorption dyes adsorption process

To ascertain the MP dye adsorption isotherm onto *Ricinus Communis*-capeed Fe_3O_4 NPs and also to determine its kinetic properties, batch adsorption tests were executed. First, 50 mL solution containing 15 mg/L concentration of MP dye was provided.

When adjustment of the initial pH of the solution was done by 0.01N HCl / 0.01N NaOH aqueous solution, no further adjustments were performed in the course of the trials. By dividing these solutions into ten samples of 50 mL, containing 0.01 g adsorbent and 15 mg/L MP dye with the help of an orbital shaker, these flasks were agitated at a steady rate of 200 rpm at room temperature. At fixed time intervals, one flask was withdrawn from the orbital shaker (1 to 15 min) and the analysis of the remaining MP dye in the sorbate solution was performed. The MP dye concentration in the solution was measured using a double beam UV–Vis spectrophotometer (Jasco, Model UV–Vis V-530, Japan) set at wavelengths 650 nm for MP dye. The amount of adsorbed dye at equilibrium (q_{max} (mg/g)) was calculated using the equation:

$$\%\ \text{Removal} = \frac{(C_0 - C_t)}{C_0} \times 100 \quad (1)$$

C_0 and C_t refer to the initial concentration of dye (mg/L), and the concentration of dye at any time (mg/L), respectively.

$$\text{qmax} = \frac{(C_0 - C_e)V}{W} \quad (2)$$

In the above equation (q_{max}) refers to the quantity of dye adsorbed onto a unit quantity of sorbent (mg/g); C_0 demonstrates the concentrations (mg/L) of dye in the primary solution and the concentrations of dyes in the aqueous phase after adsorption is demonstrated by *C*. The volume of the aqueous phase (mL) is shown by *V*, and *w* shows the weight of the sorbent (g). The evaluation of the thermodynamic properties of the adsorption process was performed by adding 0.01 g of *Ricinus Communis*-capeed Fe_3O_4 NPs into 15 mg/L initial MP dye concentration in each experiment. For 12 min at room temperature, each solution was shaken uninterruptedly. The MP dye concentration was estimated after the solution equilibrium and desorption outcomes were obtained in the present work.

Artificial neural network

In recent years in different fields of science, various applications of artificial neural network models were provided. In this research, modeling is done by MATLAB software. To identify this model, also we must introduce our data to software in normalized view [23].

Fuzzy systems based on adaptive neural networks (ANFIS)

Neural-fuzzy inference system is a multilayer adaptive network that obtained the main elements; the fuzzy system functions and their application in complex systems modeling and control have achieved tremendous success. The most common and most practical methods are the Adaptive Neural Fuzzy Inference model that was introduced by *Yang*. This model uses a hybrid algorithm and adaptive post-spreading of error for the topics of training parameters of the fuzzy system. An inference system that uses an adaptive learning algorithm is called neural fuzzy and is briefly described as ANFIS which uses a set of ANFIS input and output data that can create a fuzzy system in which the parameters of membership functions of input and output parameters are adjusted well by using a neural network algorithm of back spreading or a combination of a neural network algorithm of back spreading algorithms and least squares method; the operation of the training algorithm in ANFIS is to adjust and calculate the network parameters in order to obtain the best accordance with the data. The structure of ANFIS Model is illustrated in Fig. 2. The training or setting of these adjustable parameters is a two-step process that is known as a combined training algorithm. In this study, for each of the inputs, three Gaussian membership functions are defined and the parameters of each of them are determined by the neural network. The total number of used fuzzy rules is 3 fuzzy rules. One important capability of the fuzzy inference system is the non-linear behavior understanding [24,25].

Artificial Neural Network (ANN)

In the network, neurons are organized in several layers. These layers are the input layer, a hidden layer or layers (middle), and MLP layer of perceptron which are multilayer outputs. Each neuron is connected to all neurons in the next layer, but there are no connections between neurons in a layer. In Artificial Neural Network (ANN), feed-forward back propagation was employed as the training algorithm. The final computed data for FFBP were juxtaposed against the experimentally attained findings. Afterward, by computing and back-propagating the errors, they finally were employed for adjusting each neuron weight. A model ANN with four input layers (initial MP dye concentration, *Ricinus Communis*-capeed Fe_3O_4NPs dosage, pH, and time) was detected at epoch

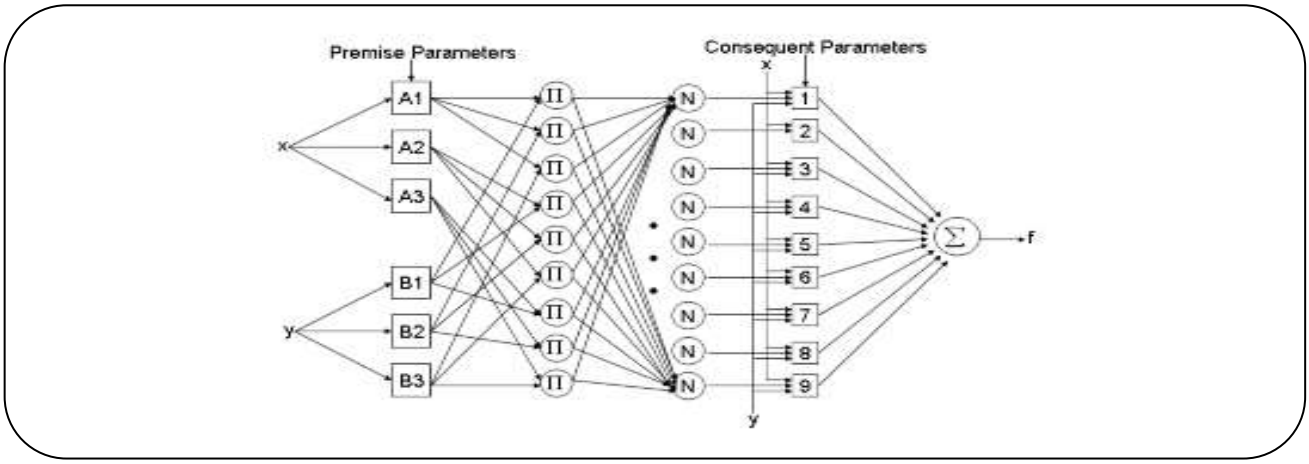

Fig. 1: The structure of ANFIS model.

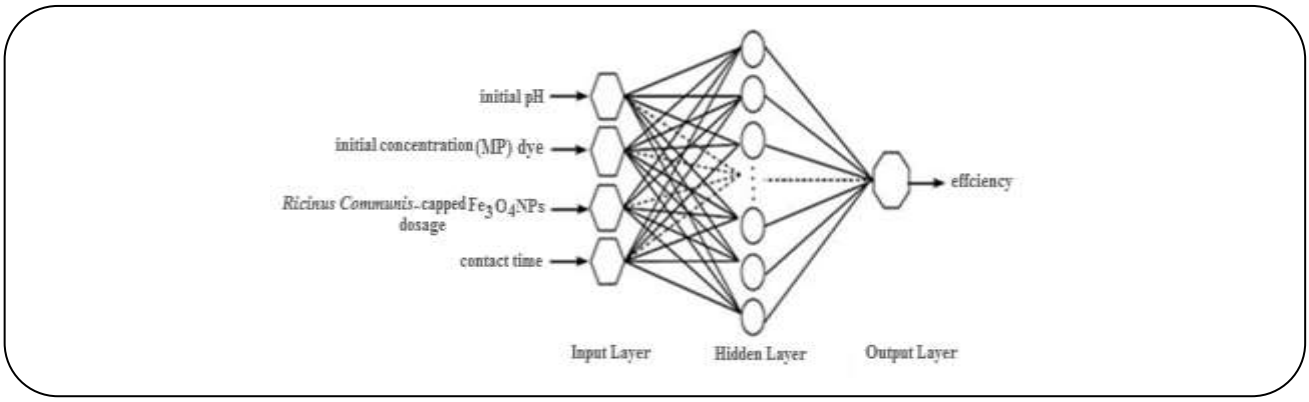

Fig. 3: Architecture of neural network system.

numbers 14, and 22 experimental points were employed to feed the model (Fig. 3). The MSE based on the function of error performance showed a minimum value at 5 neurons, from training, test, and data points, respectively and the data set was derived. In the present study, the Levenberg-Marquardt backpropagation algorithm was used for the network [25].

This algorithm accelerates attaining convergence and provides the accuracy of the results [25,26]. The tan sigmoid (Eq.(3)) and linear transfer functions were used for transfer functions in the hidden and output layers. All samples were normalized between 0-1, to achieve fast convergence, and commensurability of the scale of the input, as well as the minimal RMSE values. The normalized values of data were obtained according to Eq. (3):

$$X_{norm} = \frac{X - X_{min}}{X_{max} - X_{min}} \quad (3)$$

Where X is variable, but X_{min} and X_{max} refer to the minimum value and the maximum value, respectively.

Statistical parameters R^2, *MSE*, *SSE*, *AARE*, and *SD* are calculated through Eqs (4-7), respectively [25]. :

$$R^2 = \frac{\sum(Y_{exp,i} - Y_{model,mean})^2 - \sum(Y_{model.i} - Y_{exp,i})^2}{\sum(Y_{exp,i} - Y_{model,mean})^2} \quad (4)$$

$$MSE = \frac{\sum(Y_{model.i} - Y_{exp,i})^2}{n} \quad (5)$$

$$SSE = \sum(Y_{model.i} - Y_{exp,i})^2 \quad (6)$$

$$AARE = \frac{1}{n}\sum\left(\left|\frac{Y_{exp,i-} Y_{model.i}}{Y_{exp,i}}\right|\right) \quad (7)$$

$$SD = \sqrt{\frac{1}{n-1}\sum\left(\left|\frac{Y_{exp,i-} Y_{model.i}}{Y_{exp,i}}\right| - AARE\right)^2} \quad (8)$$

Where Mean Squared Error (MSE) and correlation coefficient (R^2).

Table 1: Characteristics of the Ricinus Communis-capeed Fe_3O_4 NPs.

Parameter	pH	Bulk density (g/mL)	Surface area (m^2/g)	Particle size range (µm)	Loss of mass on ignition
Value	7.0	0.607	250.0	45.0-250.0	0.6235

RESULTS AND DISCUSSION

Characterization of adsorbent

BET analysis of Ricinus Communis-capeed Fe_3O_4 NPs

The pore structure parameters of molecular sieve materials such as N2 adsorption-desorption isothermal curve and specific surface area were determined by a micrometric adsorption analyzer. The sample was dropped onto the slide for conducting layer treatment, at 77 K liquid nitrogen temperature and the operating voltage was 20 kV. The specific surface area was calculated using the Brunner-Emmett-Teller (BET) method. The bulk density affects the rate of adsorption of MP dye solution onto *Ricinus Communis*-capeed Fe_3O_4NPs shown in Table 1. In the present study, the bulk density was less than 2.0 indicating that the activated carbon materials are in fine nature and hence enhanced the adsorption of MP dye solution from aqueous solution. The moisture content (0.3%) was determined, even though it does not affect the adsorption power dilutes the adsorbents and therefore necessitates the use of the additional weight of adsorbents to provide the required weight [27]. The surface area of *Ricinus Communis*-capeed Fe_3O_4NPs in the present research study was (45.231 m^2/g and 1.34×10^{-2} cm^3/g).

FT-IR analysis

FT-IR spectra for *Ricinus Communis*-capeed Fe_3O_4NPs are shown in (Fig. 4). The vibrational frequencies for stretching bonds in PSF membrane molecules cannot be detected by FT-IR analysis. This confirms that *Ricinus Communis*-capeed Fe_3O_4NPs don't show any definite absorption peaks in the range 400 - 4000 cm^{-1}. The vibration modes located at 3451 cm^{-1} can be assigned to the O–H broad absorption mode due to the hydroxyl group in the compound. The absorption band at 1558 cm^{-1} is due to the O–H bending vibration from the water molecules adsorbed into the surface. The absorption band at 745 and 545 cm^{-1} is due to the Fe–O bending in the molecules adsorbed into the surface. There is a furthermore subtle point that no significant difference between the FT-IR spectra of *Ricinus Communis*-capeed Fe_3O_4NPs is observed [28].

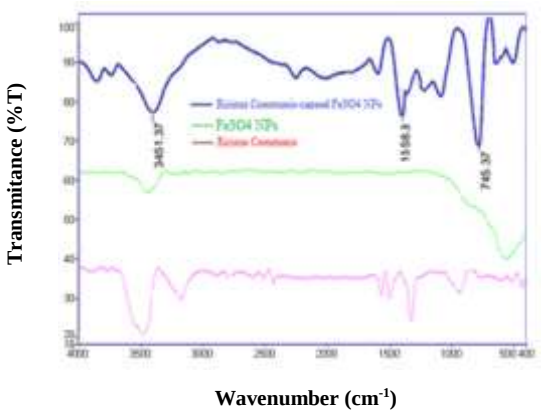

Fig. 4: FT-IR transmittance spectrum of the prepared Ricinus Communis-capeed Fe_3O_4 NPs.

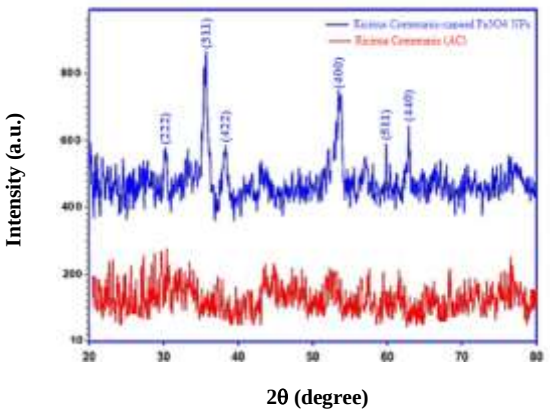

Fig. 5: X-ray diffraction of Ricinus Communis-capeed Fe_3O_4 NPs.

XRD analysis

The XRD pattern of the *Ricinus Communis*-capeed Fe_3O_4NPs (Fig. 5), represents show peaks at 2θ= 30.2°, 36.5°, 38.8°, 53.2°, 60.4°, and 62.4° belonging to the lattice planes of (222), (311), (422), (400), (511) and (440), confirm the cubic structure of *Ricinus Communis*-capeed Fe_3O_4NPs [29]. As can be seen, the entirely crystalline structure is confirmed, while the high intensity of peak at 38.8° (311) indicates the presence of a low quantities of substances in an amorphous condition.

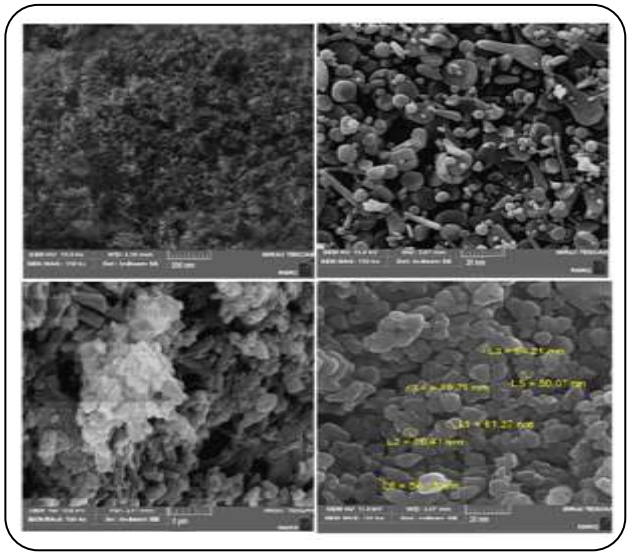

Fig. 6: The (SEM) image of the prepared Ricinus Communis-capeed Fe_3O_4 NPs.

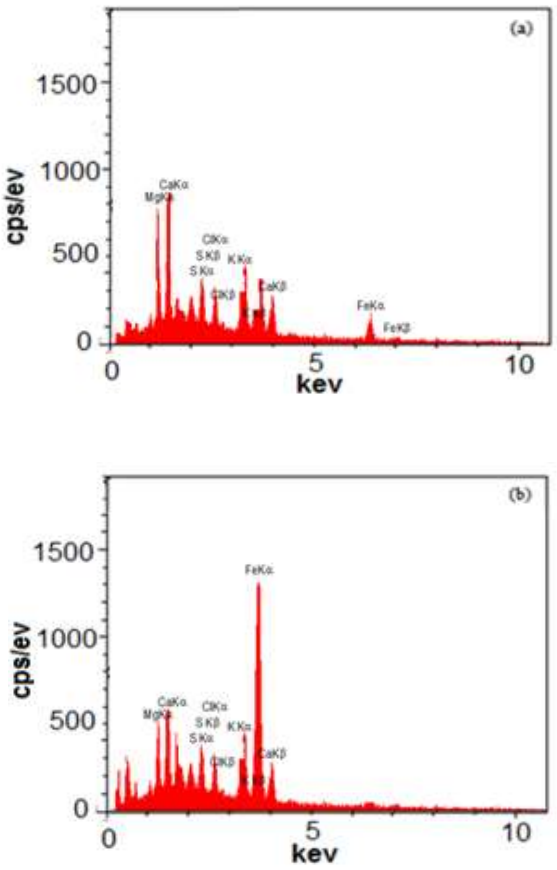

Fig. 7: (a) The EDX transmittance spectrum of the prepared Ricinus Communis and (b) The EDX transmittance spectrum of the prepared Ricinus Communis-capeed Fe_3O_4NPs.

Surface morphology

The morphological properties of *Ricinus Communis*-capeed Fe_3O_4 NPs were investigated by FE-SEM and are exhibited in (Fig. 6), the evenness, homogeneity, orderliness, and approximate uniformity of synthesized *Ricinus Communis*-capeed Fe_3O_4 NPs (even in size distribution) can be observed. *Ricinus Communis*-capeed Fe_3O_4 NPs after surface modification came to be uneven, bigger, and agglomerate**.** It can be seen that the particles are mostly spherical with various size distributions as they form agglomerates. Based on the particle size distribution, we obtained the average particle size in the range of 40-60 nm very close to those determined by XRD analysis [29].

EDX analysis

EDX (energy-dispersive X-ray spectroscopy) spectrum of (Fig. 7a) The EDX transmittance spectrum of the prepared *Ricinus Communis* and (Fig. 7b) EDX spectrum recorded from a film, after the formation of *Ricinus Communis*-capeed Fe_3O_4NPs [30].

Point of Zero Charge (PZC)

Point of Zero Charge (PZC), The pH of the *Ricinus Communis*-capeed Fe_3O_4NPs is 7.1, as presented in (Fig. 8). This value indicates that the sorbent surface can acquire a positive charge at pH <pHpzc. By contrast, the surface charge of the sorbent is negative at the solution pH of 7, indicating the capability of MP dye adsorption onto *Ricinus Communis*-capeed Fe_3O_4NPs. Enhanced electrostatic attractions may have occurred between surface functional groups in the negatively charged *Ricinus Communis*-capeed Fe_3O_4NPs when the MP dye is denoted. The pH value of the solution affects the surface charge of the adsorbent and the uptake behavior and efficiency of the adsorbent. The difference between the initial and final pH values (pH = pH in Fig. 8, the pH_{PZC}- pH_i) was plotted against the pH was noted as the pH in which the initial pH and the final pH are equal [31].

Impact of pH on the adsorption

The impact of pH value in the adsorption process is considerable. The deletion of MP dye onto sorption *Ricinus Communis*-capeed Fe_3O_4NPs as a function of pH by varied sorbent is shown in (Fig. 9). To control optimum pH for the highest deletion of MP dye, the measurement of equilibrium adsorption of MP dye was done at varied

pH levels from 1.0 to 8.0 by adjusting the initial MP dye concentrations at 15 mg/L and the summary of the obtained outcomes are displayed [32]. The highest deletion percentages of MP dye were procured at pH 7.0. Abatement in MP dye deletion at pH <7 happened due to competition of MP dye with H^+. Additionally in highly acidic pH, a sharp concentration of H^+ set the scene for the protonation of nitrogen atoms on the surface of adsorbents and provoked the reduction of interaction with MP dye and the surface of adsorbents. Both reasons precipitation of hydroxide and conversion of MP dye provoked the reduction in MP dye deletion at pH >7. This phenomenon obstructed the access of MP dye molecules to adsorption sites and culminated in less adsorption of MP dye onto sorption *Ricinus Communis*-capeed Fe_3O_4NPs [33].

Impact of the dosage of absorbent

The dosage of adsorbent is known as a significant factor in the elimination of dyes. It is related to the adsorption capacity for a known concentration of dyes. Therefore, the adsorption efficiency for MP dye was investigated as a function of the dose of adsorbent. The percentage of dyes adsorption increases sharply when the adsorbent is charged to 0.01 g, as it is seen in (Fig. 10). This finding shows that when the adsorption sites are not yet saturated at the time of the adsorption process, the availability of adsorption sites was increased by increasing the dose of adsorbent [33,34]. Therefore, 0.01 g was selected as the preferred dose of adsorbent for subsequent experiments due to the highest absorption capacity. This fact can be explained in another way the small adsorbent ratio creates less active sites for dyes to bind on the surface of *Ricinus Communis*-capeed Fe_3O_4NPs, and therefore, the sorption efficiency is low. Following the increase in sorbent dose, more active sites are provided, which increases adsorption efficiency until saturation.

Impact of the contact time on the adsorption

The contact time is an effective factor that affects considerably adsorption. Indeed, for maintaining the adsorbent/adsorbate equilibrium, it should enough prolong the contact time to setting up the equilibrium between adsorbent and adsorbate. Thus, the impact of contact time on the sorption of MP dye onto *Ricinus Communis*-capeed Fe_3O_4 NPs was examined. The removal of MP dye was scrutinized in batch experiments applying 1 to 15 min

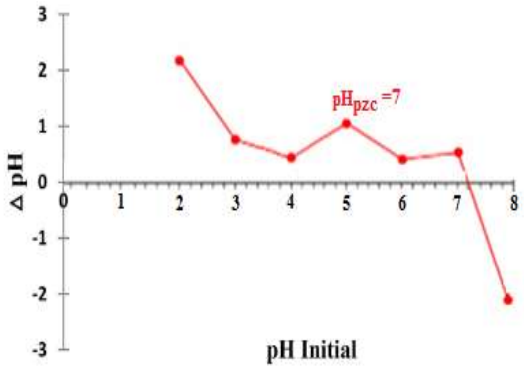

Fig. 8: pH_{pzc} of MP dye and effect of initial pH onto sorption Ricinus Communis-capeed Fe_3O_4NPs.

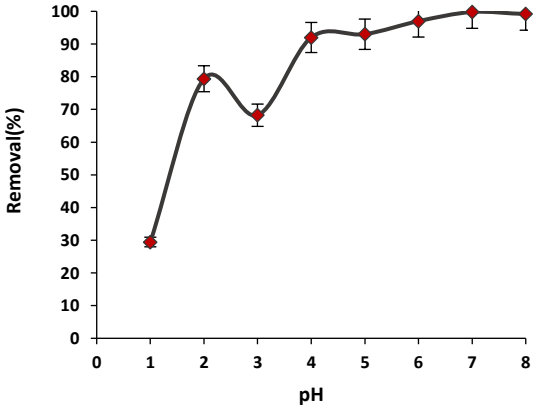

Fig. 9: Impact of initial solution pH on the sorption quantity of MP dye onto Ricinus Communis-capeed Fe_3O_4NPs [MP dye conc = 15 mg/L; adsorbent dose = 0.01g; contact time = 12 min; stirring speed = 200 rpm].

contact time, pH value 7 for MP dye (5.0, 7.5, and 15.0 mg/L), 0.01 g adsorbent dose, and room temperature. Fig. 11, shows the effect of contact time on the removal of MP dye onto *Ricinus Communis*-capeed Fe_3O_4 NPs. Based on this figure, the optimum contact time may be chosen as 12.0 min [35].

Impact of temperature

To study the effects of temperature on the adsorption of dye by *Ricinus Communis*-capeed Fe_3O_4NPs the experiments were performed at temperatures from 283.15 to 331.15 K. (Fig. 12), shows the influence of temperature of MP dye onto *Ricinus Communis*-capeed Fe_3O_4NPs is shown in Fig. 12. As it can be seen, the adsorption MP dye onto *Ricinus Communis*-capeed Fe_3O_4NPs of the process decreases

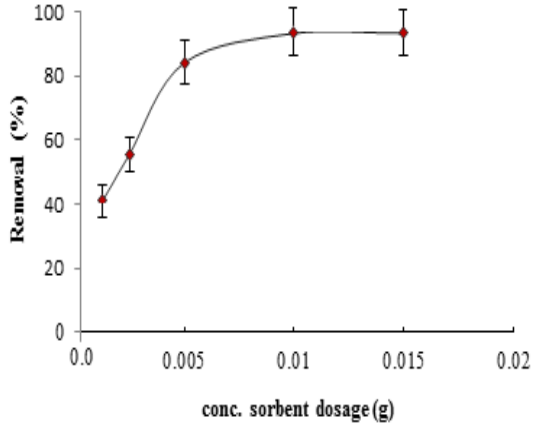

Fig. 10: Impact of dosage Ricinus Communis-capeed Fe_3O_4NPs on the adsorption quantity of MP dye. [MP dye conc = 15 mg/L; pH = 7; time = 12 min; stirring speed = 200 rpm].

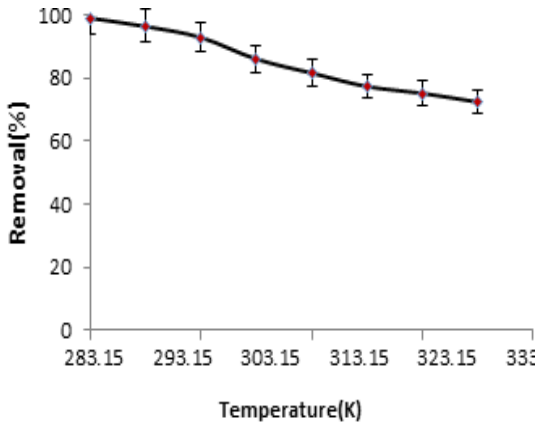

Fig.12: Impact of temperature on the sorption of MP dye by Ricinus Communis-capeed Fe_3O_4NPs [MP dye conc = 15 mg/L; pH = 7; adsorbent dose = 0.01g; time = 12 min; stirring speed = 200 rpm].

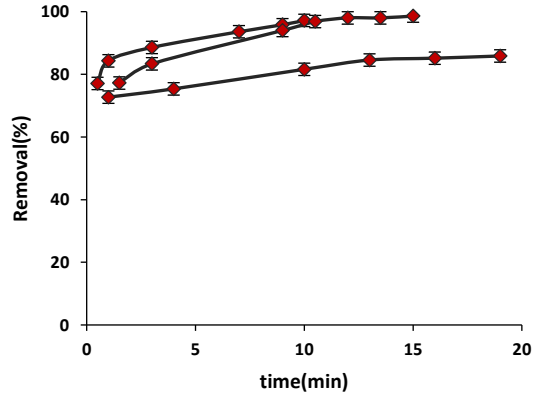

Fig. 11: Impact of contact time onto sorption of MP dye by Ricinus Communis-capeed Fe_3O_4NPs. [MP dye conc = 15 mg/L; pH = 7; adsorbent dose = 0.01g; stirring speed = 200 rpm].

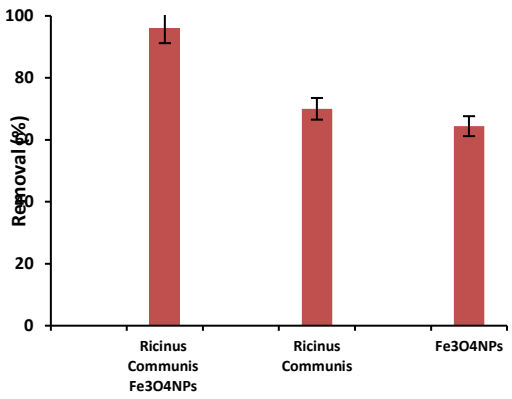

Fig. 13: **Comparison of the effectively of Fe_3O_4NPs, *Ricinus Communis*, and *Ricinus Communis*-capeed Fe_3O_4 NPs** *[MP dye conc = 15 mg/L; pH = 7; adsorbent dose = 0.01g; time = 12 min; stirring speed = 200 rpm].*

with the temperature increasing. This may have come from the fact that the adsorption process may be an endothermic one [36].

A comparative study

The adsorption percent of MB dye onto each of Fe_3O_4NPs, *Ricinus Communis*, and *Ricinus Communis*-capeed Fe_3O_4 NPs was evaluated at the optimum condition and the obtained results are represented in (Fig. 13). As can see, the trend of the effectively of mentioned adsorbents for removing MB from aqueous media as follows:

Ricinus Communis-capeed Fe_3O_4 NPs (96.0%)> *Ricinus Communis* (70.0%)> Fe_3O_4 NPs (64.4%).

Impact of concentration on the adsorption of MP dye

For this purpose, in a series of similar experiments, 50 mL of MP dye solution with concentrations different (mg/L), and 0.01 g of *Ricinus Communis*-capeed Fe_3O_4NPs, pH 7, and other variables for 12 minutes at 200 rpm, respectively, stirred at room temperature to adsorb dye on the modified activated carbon Be done with nanoparticles. The major adsorption of dye takes place at low concentrations and with increasing concentration, the percentage of adsorption decreases. Although with increasing initial concentration, the amount of adsorbed dye increases, the percentage of its removal decreases. The results are presented in Fig. 14.

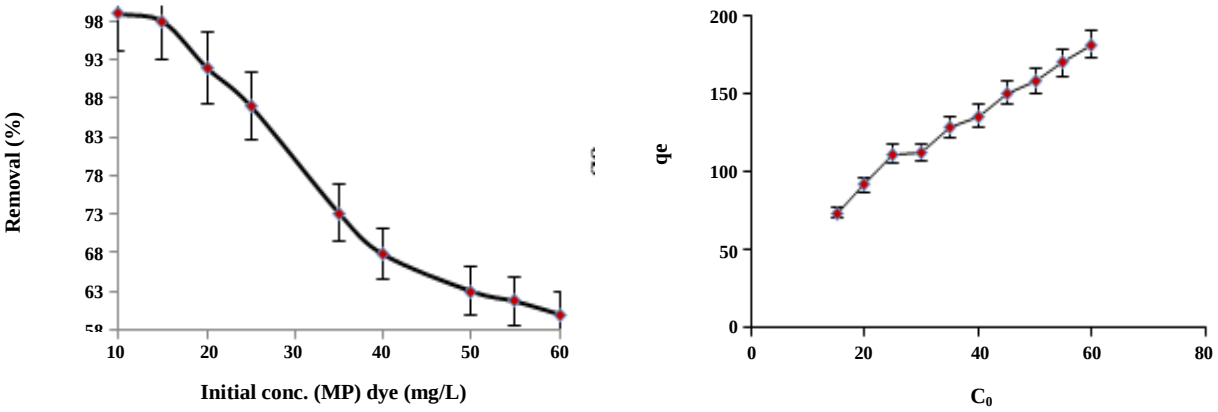

Fig. 14: Impact of concentration on the adsorption of MP dye [pH = 7; adsorbent dose = 0.01g; time = 12 min; stirring speed = 200 rpm].

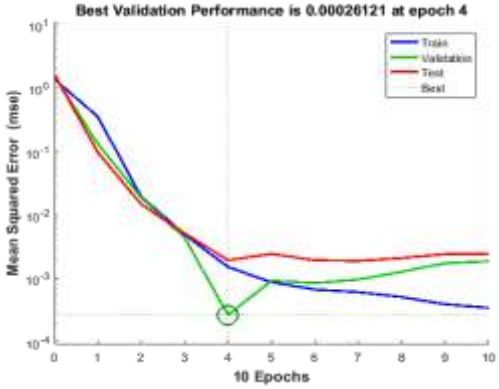

Fig. 15: gradual change of training, validation, and test errors as a function of the number of training epochs during ANN for the MP dye deletion by Ricinus Communis-capeed Fe_3O_4 NPs.

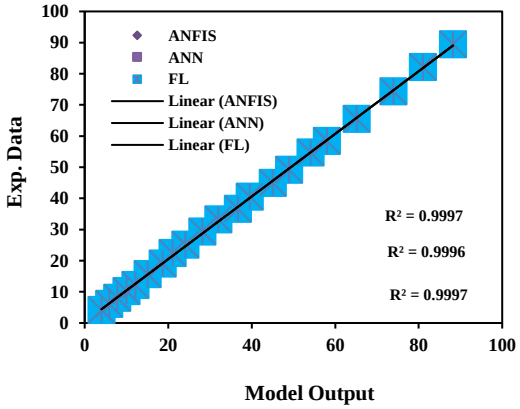

Fig. 16: The plot of error histogram Comparison of experimental values with the output of all three models for the MP dye deletion by Ricinus Communis-capeed Fe_3O_4 NPs.

Modeling of Artificial neural network process

The function of the network is under the influence of three functions weight (training), net input, and transfer (training). At epoch numbers 10 and 36 experimental points, ANN model as a tool (mean square error) MSE_{ANN} = 0.0034, MSE_{FL} = 0.023 and MSE_{ANFIS} = 0.0020 for removal of the MP dye onto *Ricinus Communis*-capeed Fe_3O_4 NPs synthesis [25,26]. The illustration of the plot of the error histogram for the sorption process in (Figs. 15 and 16) indicates that in this process the errors are extremely low. In the current study and all along the net training process, a minimum value at 5 neurons was observed for the MSE based upon the function of error performance. The appropriateness and precision of the ANN model with four input layers (namely, initial MP dye concentration, pH, adsorbent dosage, and time(min)) based upon the output layers (elimination of target compounds) was confirmed in predicting and estimating the MP dye onto *Ricinus Communis*-capeed Fe_3O_4 NPs. In Table 2, the MSE and the correlation coefficients (R^2) for training, testing, and validation in determining MP dye are presented.

It can be seen that the sum of the squares of relative error, the mean of the sum of the squares of error, the mean of the absolute error, the standard deviation, and the correlation coefficient of the findings of all three models are juxtaposed. The observed results proved the superiority of the ANFIS model neuro-fuzzy model and ANN neural network model Moreover, the obtainment of the lowest determination errors for MP dye is possible within a very short time which clearly shows the greater contribution of *Ricinus Communis*-capeed Fe_3O_4NPs in deleting MP dye.

Table 2: Statistical comparison of two models of artificial neural network.

Modeling	SSE	MSE	AARE	SD	R^2
ANN	0.1224	0.0034	0.0292	0.000328	0.9996
FL	0.0825	0.0023	0.0205	0.000263	0.9991
ANFIS	0.0732	0.0020	0.0156	0.000199	0.9999

Adsorption isotherms

The adsorbate molecules division among the solid and liquid phases in equilibrium is designated based on the isotherms of adsorption. Adsorption of MP dye onto *Ricinus Communis*-capeed Fe_3O_4NPs was modeled based on four adsorption isotherms of Freundlich, Langmuir, Temkin, and Dubinin–Radushkevich (D-R) isotherms [37].

A detailed description of the adsorption isotherm at the equilibrium state is possible based on the mathematical relevance between the (q_e) as mg/g and the non-adsorbed quantity of dyes (C_e) as mg/L at the determined temperature. For the accurate study of adsorption isotherms, the Langmuir, Freundlich, Temkin, and Dubinin–Radushkevich (D-R) models were employed (Fig. 17). Based on the Langmuir model, at homogeneous surfaces there is any interaction between the adsorbed molecules and the adsorption process. The following equation presents the Langmuir model [38]:

$$Ce/qe = 1/KLqmax + Ce/qmax \quad (9)$$

In the above equation C_e , q_e, $q_{max,}$ and K_L are equilibrium concentration (mg/L), adsorption capacity (mg/g), and a maximum of adsorption capacity (mg/g) and Langmuir constant (L/mg). The Langmuir model proved to be the best because it provides a strong correlation in all masses of adsorbent. Increasing the amount of adsorbent caused a considerable increase in the adsorbed dyes amounts (Fig. 17a). Calculation of K_F and adsorption capacity in the Freundlich model was performed from the interception and slope of the linear plot of (Fig. 17b) [39].

$$\ln qe \text{ vs. } \ln Ce \quad (10)$$

The isotherm model of Temkin (Fig. 17c) was employed to evaluate adsorption heat and interaction between adsorbent and adsorbate based on the following equation:

$$q_e = \frac{Rt}{b}\ln K_T + \frac{RT}{b}\ln C_e \quad (11)$$

In this model as mentioned above, *R, b, t, K_T,* and *T* are the universal gas constant (8.314 J/mol. K), Temkin constant, the heat of the adsorption (J/mol), the binding constant at equilibrium (L/mg) and absolute temperature (K) [32].

Dubinin–Radushkevich (D-R) isotherms: For investigated the nature of adsorption, this model is used. The linear form of this model is expressed by the following equation:

$$Lnqe = lnqm - \beta\varepsilon^2 \quad (12)$$

Where β is the activity coefficient related to mean sorption energy. (mol^2 / kJ^2), and ε is the Polanyi potential that can be calculated from bellow equation:

$$\varepsilon = RTln(1 + 1/Ce) \quad (13)$$

Where *R* and *T* are the ideal gas constant (8.3145 J/mol K) and absolute temperature (K), respectively (Fig. 17d) [33].

The slope of the plot of ln q_e versus ε^2 gives *B* and its intercept yields the Q_s value. The linear fit between the plot of C_e/q_e versus C_e and calculated correlation coefficient (R^2) for the Langmuir isotherm model shows that the dye removal isotherm can be better represented by the Langmuir model (Table 3). This confirms that the adsorption of dye takes place at specific homogeneous sites as a monolayer onto the *Ricinus Communis*-capeed Fe_3O_4 NPs.

Further discussion about Langmuir isotherm

Investigation about the adsorption uptake of MP dye was done for an initial concentration range from 5 to 15 mg/L and exhibited in (Fig. 18). The essential features of a Langmuir isotherm can be expressed in terms of a dimensionless constant separation factor or equilibrium parameter, R_L that is used to predict if an adsorption system is favorable or unfavorable [40]. Langmuir isotherm can be criticized in terms of a dimensionless constant separation factor or equilibrium parameter, R_L which is used to predict if the isotherm model is favorable or not. The R_L factor is defined as follows:

Table 3: Various isotherm constants and correlation coefficients calculated for the adsorption of MP dye by Ricinus Communis-capeed Fe_3O_4 NPs. [MP dye conc = 15 mg/L; pH = 7; adsorbent dose = 0.01g; time = 12 min; stirring speed = 200 rpm; temp = 25ºC].

Isotherm	parameters	MP dye
Langmuir	q_m (mg/g)	195.0
	K_L (L/mg)	0.455
	R^2	0.970
Freundlich	n	0.193
	K_F $(mg)^{1-n}$ L^n/g	86.1
	R^2	0.934
Temkin	B_T (J/ mol)	21.8
	K_T (L/ mg)	53.09
	R^2	0.879
Dubinin–Radushkevich (D–R)	Q_s (mg/g)	132.026
	B	5E-08
	E (kj/mol) = $1/(2B)^{1/2}$	3162.27
	R^2	0.58

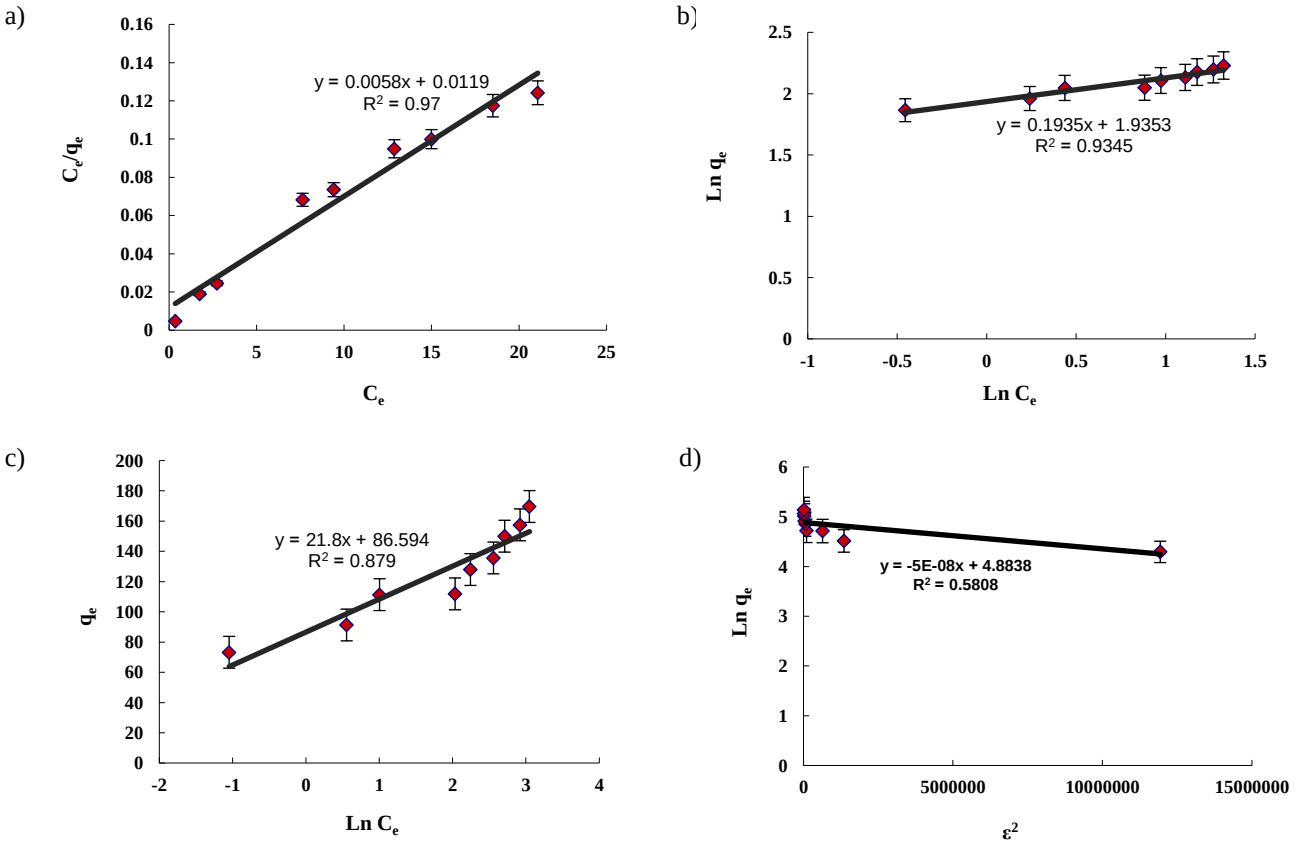

Fig. 17: (a) Langmuir isotherm (b) Frendlich isotherm (c) Temkin isotherm (d) Dubinin-Radushkevich isotherm on the sorption quantity of MP dye by Ricinus Communis-capeed Fe_3O_4 NPs. [MP dye conc = 15 mg/L; pH = 7; adsorbent dose = 0.01g; time = 12 min; stirring speed = 200 rpm].

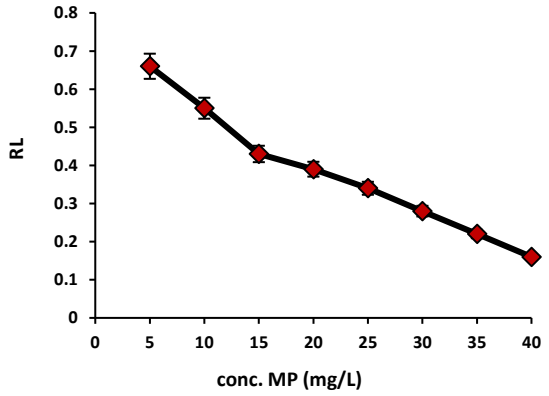

Fig. 18: Plot of R_L versus C_0, that Langmuir isotherm is favorable for representing the experimental data of the MP dye by Ricinus Communis-capeed Fe_3O_4 NPs. [MP dye conc = 15 mg/L; adsorbent dose = 0.01g; pH = 7; contact time = 12 min; stirring speed = 200 rpm].

$$R_L = \frac{1}{1 + K_L C} \quad (14)$$

The values of R_L can illustrate the shape of the isotherm to be either unfavorable (R_L>1), linear (R_L=1), favorable (0<R_L<1), or irreversible (R_L=0). The plot of the calculated R_L values versus the initial concentration of MP dye is shown in Fig.. 18, indicating that the Langmuir adsorption isotherm is fairly suitable for MP adsorption onto *Ricinus Communis*-capeed Fe_3O_4NPs adsorbent.

The adsorption kinetics survey

Adsorption of a solute by a solid in an aqueous solution through complex stages [41], is strongly influenced by several parameters related to the state of the solid (generally with the very heterogeneous reactive surface) and to physic-chemical conditions under which the adsorption occurred. The rate of dye adsorption onto adsorbent was fitted to traditional models like pseudo-first and pseudo- second-models. The Lagergren pseudo-first-order model scribed the adsorption kinetic data. The Lagergren is commonly expressed as follows:

$$\frac{dq_t}{dt} = k_1(q_e - q_t) \quad (15)$$

Where q_e and q_t(mg/g) are the adsorption capacities at equilibrium and at time *t*, respectively. k_1 is the rate constant of the pseudo-first-order adsorption(L/min). The log (q_e−q_t) versus t was plotted and the values of k_1 and q_e were determined by using the slope and intercept of the line, respectively [42].

$$\log(q_e - q_t) - \log q_t - \left(\frac{k_1}{2.303}\right)t \quad (16)$$

The fact that the intercept is not equal to q_e implies that their action is unlikely to follow the first order. The relationship between initial solute concentration and rate of adsorption is linear when pore diffusion limits the adsorption process. Therefore, it is necessary to fit experimental data to another model (Table 4) such as the pseudo-second-order model [43], based on the following equation:

$$\frac{dq_t}{dt} = k_2(q_e - q_t)^2 \quad (17)$$

Eq.(13) is integrated over the interval 0 to t for t and 0 to $q_t$for q_t, to give

$$\frac{t}{q_t} = \frac{1}{k_2 q_e^2} + \frac{t}{q_e} \quad (18)$$

As mentioned above, the plot of log (q_e−q_t) versus t does not show good results for the entire sorption period, while the plot of t/q_t versus t shows a straight line. The values of k_2 and equilibrium adsorption capacity (q_e) were calculated from the intercept and slope of the plot of t/q versus t (Table 4). The calculated q_e values at different working conditions like various initial dyes concentrations and/or adsorbent masses were close to the experimental data and higher R^2 values corresponding to this model confirm its more suitability for the explanation of experimental data [42-44]. This indicates that the pseudo-second-order kinetic model applies better for the adsorption of MP dye system for the entire sorption period. The kinetic data from pseudo-first and pseudo-second-order adsorption kinetic models given in Table 4. The linear plots of t/q_t versus t indicated a good agreement between the experimental and calculated q_e values for different initial dye concentrations. Furthermore, the correlation coefficients of the pseudo-second-order kinetic model ($R^2 = 0.9996$) were greater than that of the pseudo-first-order model (R^2= 0.9444) for MP dye respectively. As a result, the adsorption fits the pseudo-second-order better than the pseudo-first-order kinetic model.

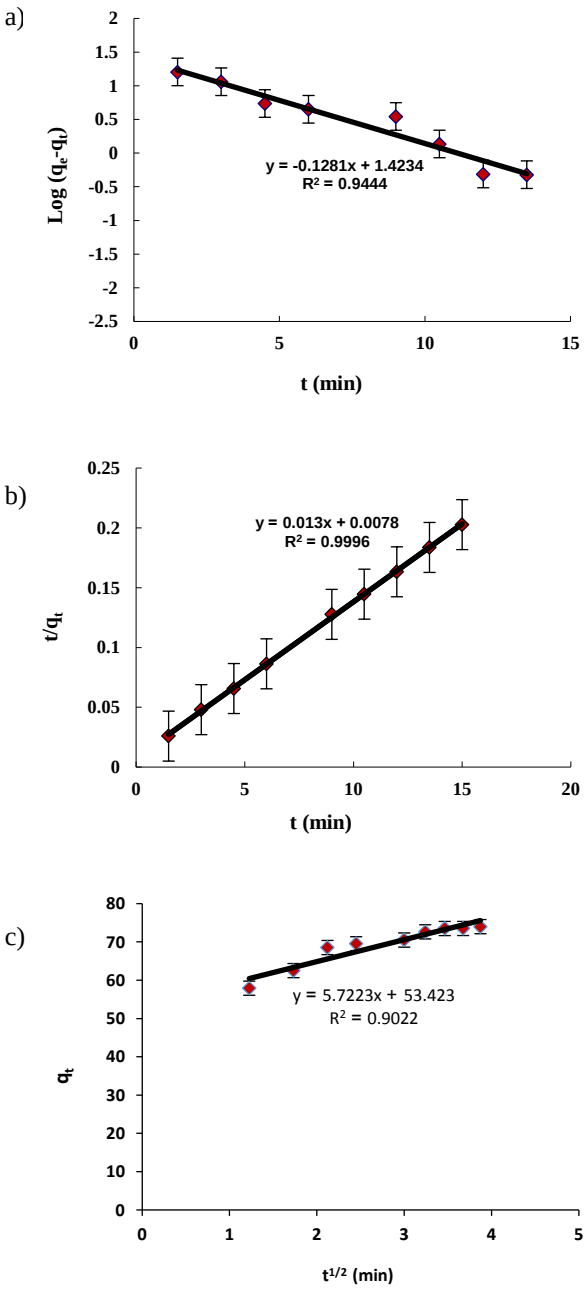

Fig. 19: (a) pseudo-first-order kinetic model (b) pseudo-second-order kinetic model (c) Intra-particle diffusion model kinetics for the adsorption of MP dye onto Ricinus Communis-capeed Fe_3O_4 NPs.

Adsorption thermodynamics

For the adsorption processes, 3 thermodynamic parameters of 1-Gibbs free energy change (ΔG°), 2- enthalpy change (ΔH°), and 3- entropy change ΔS° were considered. Their computation becomes possible by utilizing the ensuing equations [45]:

$$\Delta G° = -RT\, lnK_{ad} \quad (19)$$

$$\ln K_{ad} = \frac{-\Delta H^{\circ}}{RT} + \frac{\Delta S^{\circ}}{R} \quad (20)$$

From a plot of lnKe against 1/T, a graph (Fig. 20) is provided. By considering the slope of this graph ΔG can be acquired. In Table 5, the summary of the thermodynamic parameter outcomes for the adsorption of MP dye onto *Ricinus Communis*-capeed Fe_3O_4NPs at diverse temperatures is demonstrated.

The estimation of ΔG^o values became possible *via* employing the equation adsorption of MP dye. As can be seen in (Fig. 20), with any increase in the temperature from 283.15 to 331.15 K, a steep reduction in the *Ricinus Communis*-capeed Fe_3O_4 NPs adsorbent was observed which confirms the endothermicity nature of the process. The thermodynamic parameters such as free energy (ΔG^0), enthalpy (ΔH^0), and entropy (ΔS^0) of adsorption. The value of (ΔG^o, ΔH^o, and ΔS^o) confirmed the sorption process was endothermic reflecting the affinity of *Ricinus Communis*-capeed Fe_3O_4NPs for removing MP dye process requires heat [46,47].

Recycling of the Adsorbent

The ability to recover and reusing of the adsorbent was tested in several steps of adsorption and desorption. The result is shown in (Fig. 21). As shown in Figure 98 % of MP dye was desorbed from the adsorbent after the first cycle and after 6 cycles, there were slight changes in MP dye desorption [48]. So, it was concluded that the desired removal of 98% can be achieved after 6 cycles.

Comparison for the amount of MP dye removed with other adsorbents

Table 6, demonstrates the max adsorption capacities of varied adsorbents for the deletion of MP dye comparatively. The type and density of active sites in adsorbents which are responsible for adsorption of metal ions from the solution result in the variation in (q_{max}) values. The outcomes of the table clearly show that the sorption capacity of utilized *Ricinus Communis*-capeed Fe_3O_4NPs in the current study is significantly high. In general, morphology, particle size and distribution, and surface structure of this sorbent were effective in its successful outcomes.

Table. 4: Kinetic parameters for the adsorption for the adsorption of MP dye onto Ricinus Communis-capeed Fe_3O_4NPs. [MP dye conc = 15 mg/L; pH = 7; adsorbent dose = 0.01g; time = 12 min; stirring speed = 200 rpm].

Model	Parameters	Value of parameters For MP dye
pseudo-First-order kinetic $\log(q_e - q_t) = \log(q_e) - (\frac{k_1}{2.303})t$	q_m (mg/g)	0.295
	K_1 (1/min)	26.485
	R^2	0.944
pseudo-Second-order kinetic $t_{/q_t} = \frac{1}{k_2 q_e 2} + \left(\frac{1}{q_e}\right) t$	q_m (mgg^{-1})	0.024
	K_2 (g/mg min)	76.92
	R^2	0.999
intra-particle diffusion $q_t = k_{intra}(t)^{1/2} + C$	K_i ((mg/g) / min)	0.143
	C (Å)	43.18
	R^2	0.902

Table. 5: The thermodynamic parameters for the adsorption of MP dye onto Ricinus Communis-capeed Fe_3O_4 NPs. [MP dye conc = 15 mg/L; pH = 7; adsorbent dose = 0.01g; time = 12 min; stirring speed = 200 rpm].

MP dye (15mg/L)	T (^{O}K)	K_C	value of ΔG^o(kJ/mol)	value of ΔH^o(kJ/mol)	value of ΔS^o (kJ/mol K)
Sorbent *Ricinus Communis*-capeed Fe_3O_4NPs	283	3.33	-2832.4	59.58	221.15
	293	12.32	-6120.2		
	303	16.75	-7103.8		
	313	26.92	-8573.0		
	323	120.60	-12875.8		
	331	157.33	-14010.7		

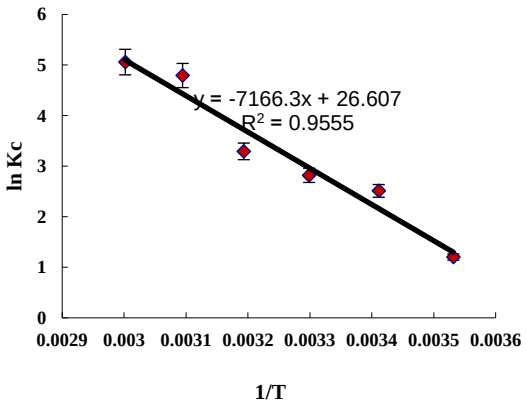

Fig.20: Plot of ln Kc vs. 1/T for the estimation of thermodynamic parameters for the adsorption of MP dye onto Ricinus Communis-capeed Fe_3O_4 NPs. [MP dye conc = 15 mg/L; pH = 7; adsorbent dose = 0.01g; time = 12 min; stirring speed = 200 rpm].

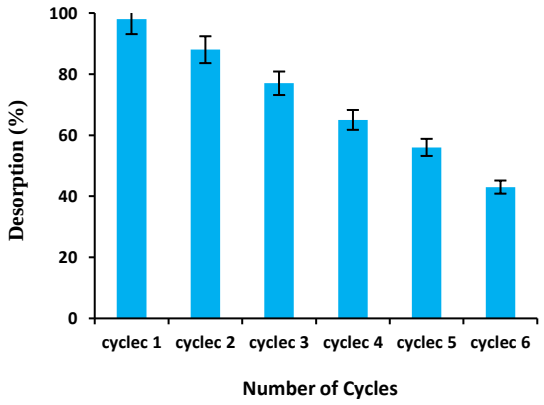

Fig. 21: Desorption of MP dye onto Ricinus Communis-capeed Fe_3O_4NPs. [MP dye conc = 15 mgL^{-1}; pH = 7; adsorbent dose = 0.01g; time = 12 min; stirring speed = 200 rpm].

Table. 6: Comparison for the amount of MP dye removed by different adsorbents.

dye	Adsorbent	Adsorption capacity (mg/g)	References
MP dye	MWTACC	85.9	[5]
MP dye	Fe_3O_4@SiO_2-NH_2	75.0	[11]
MP dye	G-Fe_3O_4	20.69	[19]
MP dye	N-doped G-NiO	3.12	[20]
MP dye	Activated carbon (AC)	7.52	[49]
MP dye	*Ricinus ommunis*-capeed Fe_3O_4NPs	195.0	Present study

CONCLUSIONS

The selection of *Ricinus Communis*-capeed Fe_3O_4NPs as an efficacious adsorbent for the deletion of MP dye from aqueous solutions has been scrutinized. In this current article, the applicability of *Ricinus Communis*-capeed Fe_3O_4NPs as an available, useful, and affordable material for deleting MP dye from aqueous media has been confirmed. With the help, the impacts of process variables including dye concentration, pH, adsorbent mass, and contact time on the adsorption of MP dye came under scrutiny. Under the conditions of pH of 7.0, MP dye concentration equal to 15 mg/L, adsorbent mass of 0.01, and sonication time of 12.0 min, the adsorption of MP dye onto *Ricinus Communis*-capeed Fe_3O_4NPs was almost 99.8%. The experimental removal efficiency of *RicinusCommunis*-capeed Fe_3O_4NPs nanoparticles got to (R^2= 0.9992) for MP dye at optimal adsorption conditions. To build up an empirical model, the neural network model was employed that based on the observed results proved to be a very potent device in determining the relative mean square error (MSE), relative error, the mean of the sum of the squares of error, the mean of the absolute error, the standard deviation and the correlation coefficient. The results of the relative superiority of the ANFIS model neuro-fuzzy model and ANN neural network model were confirmed. The results of these three models' surveys show that in modeling by using artificial nerve networks in At epoch numbers 10 and 36 experimental points and tension transmission function and the number of 25 neurons in each layer, has the least error rate and the most correlation coefficient equal to 99 percent and the least possible error in simulation with artificial nerve network equal, ANN model as a tool (mean square error) MSE_{ANN} = 0.0034, MSE_{FL} = 0.023 and MSE_{ANFIS} = 0.0020, THEn the other simulated models. The excellent contribution of *Ricinus Communis*-capeed Fe_3O_4 NPs in deleting MP dye was confirmed when the lowest errors were obtained in no time. Equilibrium adsorption revealed that the system followed the Langmuir model. The highest adsorption capacity value of MP dye with *Ricinus Communis*-capeed Fe_3O_4 NPs was observed to be (195.0 mg/g). The kinetics studies brought to light that MP dye deletion followed pseudo-second-order rate equation. Thermodynamic parameters of free energy (ΔG^0), enthalpy (ΔH^0), and entropy (ΔS^0) of adsorption were determined using isotherms. ΔG^0 = -2.8324 kJ/mol, ΔH^0 = 59.58 kJ/mol, and ΔS^0 = 221.15 kJ/mol.K. The value of (ΔG^o, ΔH^o, and ΔS^o) confirmed the sorption process was endothermic reflecting the affinity of *Ricinus Communis*-capeed Fe_3O_4NPs for removing MP dye process requires heat. In summary, the results of this research show that artificial nerve network systems and phasic systems on the basis of comparative nerve networks, in predicting different parameters. The findings proved the appropriateness of the present procedure for the successful deletion of methylparaben MP dye from an aqueous solution, and also, it can be used as an intelligent tool Investigations on the suitability of this adsorbent for the deletion of other materials have been suggested.

Abbreviations

MP	Methyl Paraben
AC	Activated carbon
BET	Brunauer–Emmett–Teller
FT-IR	Fourier Transform InfraRed
XRD	X-ray diffraction
EDX	Energy-dispersive X-ray analyzer
SEM	Scanning electron microscopy
C	Initial concentration of dye
Ce	Equilibrium concentration of dye

cm^{-1}	One per centimeter
g	Gram
K	Kelvin
mg/L	Milligram per liter
W	Weight
T	Temperature
t	Time
V	Volume
min	Minutes
mL	Milliliter
mg/g	Milligram per gram
R^2	Coefficient of determination
m^2/g	Meter square per gram
nm	Nanometer
^0C	Celsius
qe	Amount of dye adsorbed at equilibrium
qt	Amount of dye adsorbed at time
qm	Adsorption capacity
R	Gas constant
K_L	Langmuir constant
K_F	Freundlich constant
k_1	Rate constant of pseudo-first order
K_2	Rate constant of pseudo-second order
ANN	Artificial neural network
FL	Neuro-fuzzy
MSE	Mean square error
SSE	Standard square error
AARE	Absolute average relative error
SD	Standard deviation

Acknowledgments

The authors gratefully acknowledge the support of this work by Omidiyeh Branch, Islamic Azad University, Iran, for their partial support of this work.

Received : May. 19, 2021 ; Accepted : Aug. 16, 2021

REFERENCES

[1] Zubair Z., Ihsanullah I., Jarrah N., Khalid A., Manzar M.S., Kazeem T.S., Al- Harthi M.A., Starch-NiFe-Layered Double Hydroxide Composites: Efficient Removal of Methyl Orange from Aqueous Phase, *J. Molecular Liquids.*, **249**: 254-264 (2018).

[2] Ihsanullah I., Jamal A., Ilyas M., Zubair M., Khan G., Atieh M.A., Bioremediation of Dyes: Current status and Prospects, *J. Water. Process. Engineering*, **38**: 101680 (2020).

[3] Jawad A.H., Abdulhameed A.S., Mastuli M.S., Acid-Factionalized Biomass Material for Methylene Blue Dye Removal: A Comprehensive Adsorption and Mechanism Study, *J. Taibah, Univ. Sci.,* **14(1)**: 305–313 (2020).

[4] Jawad A.H., Abdulhameed A.S., Statistical Modeling of Methylene Blue Dye Adsorption by High Surface Area Mesoporous Activated Carbon from Bamboo Chip Using KOH-Assisted Thermal Activation, *Energ. Ecol. Environ.,* **5(5)**: 1-18 (2020).

[5] Geaneth Pertunia Mashile G., Azile Nqombolo A.M., Mogolodi Dimpe K., Philiswa N., Nomngongo N., Recyclable Magnetic Waste Tyre Activated Carbon-Chitosan Composite as an Effective Adsorbent Rapid and Simultaneous Removal of Methylparaben and Propylparaben from Aqueous Solution and Wastewater, *J. Water. Process Engineering.,* **33**: 101011 (2020).

[6] Pargari M., Marahel F., Mombini Godajdar B., Ultrasonic Assisted Adsorption of Propyl Paraben on Uultrasonically Synthesized TiO_2 Nano Particles Loaded on Activated Carbon: Optimization, Kinetic and Equilibrium Studies, *Desal. Water Treat.,* **212**: 164-172 (2021).

[7] Md Yusoff M., Yahaya N., Md Saleh N., Raoov M., A Study on the Removal of Propyl, Butyl, and Benzyl Parabens *via* Newly Synthesised Ionic Liquid Loaded Magnetically Confined Polymeric Mesoporous Adsorbent, *RSC. Adv*. **8**: 25617–25635 (2018).

[8] An J., Xia Ch., He J., Feng H., Oxidation of Propyl Paraben by Ferrate (VI): Kinetics, Products, and Toxicity Assessment, *J. Environ. Sci. Health. A.*, **53(10)**: 873-882 (2018).

[9] Habbal S., Haddou B., Cansellier J., Easy Removal of Methylparaben and Propylparaben from Aqueous Solution Using Nonionic Micellar System, *Tenside Surfactants Detergents.,* **56(2)**: 112-118 (2019).

[10] Yegane Badi M., Fallah S., Rezaei Nia S., Esrafili A., Monitoring of Para-Hydroxy Benzoic Acid Esters (Antimicrobial and Preservative) in Tehran Wastewater Treatment Plants and Performance Evaluation of Various Wastewater Treatment Method in the Removal of These Compounds, *J. Environ. Health. Eng.,* **3(4)**: 259-269 (2016).

[11] Mohammadi F., Esrafili A., Sobhi H.R., Behbahani M., Kermani M., Asgari E., Rostami Fasih Z., Evaluation of Adsorption And Removal of Methylparaben from Aqueous Solutions Using Amino-Functionalized Magnetic Nanoparticles as an Efficient Adsorbent: Optimization and Modeling by Response Surface Methodology (RSM), *Desal. Water Treat.*, **103**: 248–260 (2018).

[12] Jawad A.H., Firdaus Hum N.N.M., Abdulhameed A.S., Mohd Ishak M.Z., Mesoporous Activated Carbon from Grass Waste via H_3PO_4-Activation for Methylene Blue Dye Removal: Modelling, Optimisation, and Mechanism Study, *Int. J. Environ. Anal. Chem.*, **99**: 1-20 (2020).

[13] Jawad A.H., Abdulhameed A.S., Surip S.V., Sabar S., Adsorptive Performance of Carbon Modified Chitosan Biopolymer for Cationic Dye Removal: Kinetic, Isotherm, Thermodynamic, and Mechanism Study, *Int. J. Environ. Anal. Chem.*, **99**_ 1-18 (2020).

[14] Abdulhameed A.S., Firdaus Hum N.N.M., Rangabhashiyam S., Jawad A.H., Wilson L.D., Yaseen Z.M., Al-Kahtani A.A., ALOthman Z.A., Statistical Modeling and Mechanistic Pathway for Methylene Blue Dye Removal by High Surface Area and Mesoporous Grass-Based Activated Carbon Using K_2CO_3 Activator, *J. Environ. Chem. Eng.*, **9**: 105530 (2021).

[15] Jawad A.H., Abdulhameed A.S., Statistical Modeling of Methylene Blue Dye Adsorption by High Surface Area Mesoporous Activated Carbon From Bamboo Chip Using KOH-Assisted Thermal Activation, *Energ. Ecol. Environ.*, (2020).

[16] Ahmadi S.H., Davar P., Manbohi A., Adsorptive Removal of Reactive Orange 122 from Aqueous Solutions by Ionic Liquid Coated Fe_3O_4 Magnetic Nanoparticles as an Efficient Adsorbent, *Iran. J. Chem. Chem. Eng (IJCCE).*, **35**: 63-73 (2016).

[17] Reghioua A., Barkat D., Jawad A.H., Abdulhameed A.S., Al-Kahtani A.A., ALOthman Z.A., Parametric Optimization by Box–Behnken Design for Synthesis of Magnetic Chitosan-Benzil/ZnO/Fe_3O_4 Nanocomposite and Textile Dye Removal, *J. Environ. Chem. Eng.*, **9**: 105166 (2021).

[18] Reghioua A., Barkat D., Jawad A.H., Abdulhameed A.S., Khan M.R., Synthesis of Schiff's base Magnetic Crosslinked Chitosan-Glyoxal/ZnO/Fe_3O_4 Nanoparticles for Enhanced Adsorption of Organic Dye: Modeling and Mechanism Study, *Sustaina. Chem. Pharmac.*, **20**: 100379 (2021).

[19] Chen H.W., Chiou C.S., Wu Y.P., Chang C.H., Lai Y.H., Magnetic Nanoadsorbents Derived from Magnetite and Graphene Oxide for Simultaneous Adsorption of Nickel Ion, Methylparaben, and Reactive Black 5, *Desal. Water Treat.*, **224**: 168-177 (2021).

[20] Husein D.Z., Facile One-Pot Synthesis of Porous N-Doped Graphene Based NiO Composite for Parabens Removal from Wastewater and Its Reusability, *Desal. Water Treat.*, **166**: 211-221 (2021).

[21] Manohar R., Shrivastava V.S., Adsorption removal of Carcinogenic Acid Violet19 Dye from Aqueous Solution by Polyaniline-Fe_2O_3 Magnetic Nano-Composite, *J. Mater. Environ. Sci.*, **6**: 11-21 (2015).

[22] Mandel K., Hutter F., Gellermann C., Sextl G., Synthesis and Stabilisation of Superparamagnetic Iron Oxide Nanoparticle Dispersions, *J. Colloids and Surfaces A: Physicochemical and Engineering Aspects.*, **390**: 173-178 (2011).

[23] Kiani K., Bagheri S., Karachi N., Alipanahpour Dil E., Adsorption of Purpurin Dye from Industrial Wastewater Using Mn-Doped Fe_2O_4 Nanoparticles Loaded on Activated Carbon, *J. Desal. Water. Treat.*, **60**: 1-8 (2019).

[24] Wong Y.J, Arumugasamy S.K., Chung C.H., Selvarajoo A., Sethu V., Comparative Study of Artificial Neural Network (ANN), Adaptive Neuro-Fuzzy Inference System (ANFIS) and Multiple Linear Regression (MLR) for Modeling of Cu(II) Adsorption from Aqueous Solution Using Biochar Derived from Rambutan (Nephelium lappaceum) Peel, *Environ Monit Assess.*, **192(7)**: 439 (2020).

[25] Jamshidi B., Tahmasebi Birgani Y., Jorfi S., Takdastan A., Dehvari M., Jamshidi B., Adsorption of Humic Acid from Aqueous Solutions onto Shellfish Ash: Kinetic and Isotherm Studies and Artificial Neural Network Modeling, *J. Environ. Health Engine. Manage.*, 7(4): 219-228 (2020).

[26] Marahel F., Mombini Godajdar B., Niknam L., Faridnia M., Pournamdari E., Mohammad Doost S., Ultrasonic Assisted Adsorption of Methylene Blue Dye and Neural Network Model for Adsorption of Methylene Blue Dye by Synthesized Mn-Doped PbS Nanoparticles. *Int. J. Environ. Anal. Chem.*, **101(5)**: 1-22 (2021).

[27] Dehghanpoor Frashah A., Hashemian S., Tamadon F., Ag Doped Hydroxyapatite Nano Particles for Removal of Methyl Red Azo Dye from Aqueous Solutions Kinetic and Thermodynamic Studies, *Eur. J. Anal. Chem.*, **15**: 32-44 (2020).

[28] Lu A.H., Schuth F., Magnetic Nanoparticles: Synthesis, Protection, Functionalization, and Application, *Angewandte Chemie International Edition.*, **46**: 1222-1244 (2007).

[29] Bagheri S., Aghaei H., Ghaedi M., Asfaram A., Monajemi M., Bazrafshan A.A., Synthesis of Nanocomposites of Iron Oxide/Gold (Fe_3O_4/Au) Loaded on Activated Carbon and their Application in Water Treatment by Using Sonochemistry: Optimization Study, *Ultrasonics – Sonochemistry.*, **41**: 279–287 (2018).

[30] Naushad M., Gaurav Sharma Zeid G., Alothman A., Photodegradation of Toxic Dye Using Gum Arabic-Crosslinkedpoly (acrylamide)/$Ni(OH)_2$/FeOOH Nanocomposites Hydrogel, *J. Clean. Production.*, **241**: 112863 (2019).

[31] Abd Malek N.N., Jawad A.H., Abdulhameed A.S., Ismail K., Hameed B.H., New Magnetic Schiff's Base-chitosan-glyoxal/fly ash/Fe_3O_4 Biocomposite for the Removal of Anionic Azo Dye: An Optimized Process, *Int. J. Biolog. Macromolecules.*, **146**: 530–539 (2020).

[32] Marahel F., Adsorption of Hazardous Methylene Green Dye from Aqueous Solution onto Tin Sulfide Nanoparticles Loaded Activated Carbon: Isotherm and Kinetics Study, *Iran. J. Chem. Chem. Eng. (IJCCE)*, **38(5)**: 129-142 (2019).

[33] Bouroumand Sh., Marahel F., Khazali F., Removal of Yellow HE4G dye from Aqueous Solutions Using synthesized Mn-doped PbS (PbS:Mn) Nanoparticles, *Desal. Water Treat.*, **223**: 388-392 (2021).

[34] Rashidi Nodeh H., Sereshti H., Ataolahi S., Toloutehrani A., Talesh Ramezani A., Activated Carbon Derived From Pistachio Hull Biomass for the Effective Removal of Parabens from Aqueous Solutions: Isotherms, Kinetics, and Free Energy Studies, *Desal. Water Treat.*, **201**: 155–164 (2020).

[35] Kaboudin B., Torabi Momen M., Kazemi F., Ray P., Novel ß-Cyclodextrin Functionalized Core-Shell Fe_3O_4 Magnetic Nanoparticles for the Removal of Toxic Metals from Water, *Anal. Chem.*, (2021).

[36] Maghami F., Abrishamkar M., Mombeni Goodajdar B., Hossieni M., Simultaneous Adsorption of Methylparaben and Propylparaben Dyes from Aqueous Solution Using Synthesized *Albizia lebbeck* Leaves-Capped Silver Nanoparticles, *Desal. Water Treat.*, **223**: 388-392 (2021).

[37] Arora C., Soni S., Sahu S., Mittal J., Kumar P., Bajpai P.K., Iron Based Metal Organic Framework for Efficient Removal of Methylene Blue Dye from Industrial Waste, *J. Molecular Liquids.*, **284**: 373-352 (2019).

[38] Yang Y., Xie Y., Pang L., Li M., Song X., Wen J., Zhao H., Preparation of Reduced Graphene Oxide/Poly(Acrylamide) Nanocomposite and Its Adsorption of Pb^{2+} and Methylene Blue, *Langmuir.*, **29**: 10727-10736 (2013).

[39] Mahini R., Esmaeili H., Foroutan R., Adsorption of Methyl Violet From Aqueous Solution Using Brown Algae Padina Sanctae-Crucis, *Turk. J. Biochem.*, **24**: 1-12 (2018).

[40] Haghdoost G.H., Removal of Reactive Red 120 from Aqueous Solutions Using Albizia lebbeck Fruit (Pod) Particle as a Low Cost Adsorbent, *J. Phys. Theore. Chem.*, **15(3,4)**: 141-148 (2019).

[41] Absalan G., Bananejad A., Ghasemi M., Removal of Alizarin Red and Purpurin from Aqueous Solutions Using Fe_3O_4 Magnetic Nanoparticles, *Anal. Bioanal. Chem. Res.*, **4**: 65-77 (2017).

[42] Fu J., Chen Z., Wang M., Liu S., Zhang J., Han R., Xu Q., Adsorption Of Methylene Blue by a High-Efficiency Adsorbent (Poly Dopamine Micro Spheres): Kinetics, Isotherm, Thermodynamics and Mechanism Analysis, *Chem. Eng. J.*, **259**: 53-61 (2015).

[43] Hubbe M., Azizian S., Douven S., Implications of Apparent Pseudo-Secound-Order Adsorption Kinetics onto Cellulosic Materials: A Review, *Bio Resources.*, **14(3)**: 7582-7626 (2019).

[44] Toor M., Jin B., Adsorption Characteristics, Isotherm, Kinetics, and Diffusion of Modified Natural Bentonite for Removing Diazo Dye, *Chem. Eng. J.*, **187**: 79-88 (2012).

[45] Bouaziz F., Koubaa M., Kallel F., Ghorbel R.E., Chaabouni S.E., Adsorptive Removal of Malachite Green from Aqueous Solutions by Almond Gum: Kinetic Study and Equilibrium Isotherms, *Int. J. Biolog. Macromolecules.*, **105**: 56-65 (2017).

[46] Banerjee S., Sharma G.C., Gautam R.K., Chatto Padhyaya M.C., Upadhyay S.N., Sharma Y.C., Removal of Malachite Green, a Hazardous Dye from Aqueous Solutions Using Avena Sativa (oat) Hull as a Potential Adsorbent, *J. Mol. Liquids.*, **213**: 162-172 (2016).

[47] Atheba P., Guadi N., Allou B., Drogui P., Trokourey A., Adsorption Kinetics and Thermodynamics Study of Butylparaben on Activated Carbon Coconut Based, *J. Encapsul. Adsorpt. Sci.*, **8**: 39-57 (2018).

[48] Mousavi E., Geramizadegan A., Adsorption of Benzyl Paraben Dye from Aqueous Solutions Using synthesized Mn-doped PbS (PbS:Mn) nanoparticles, *J. Phys. Theore. Chem.*, **17**(3,4): 123-143 (2020).

[49] Chin Y.P., Mohamad S., Bin Abas M.R., Removal of Parabens from Aqueous Solution Using ß-cyclodextrin Cross-Linked Polymer, *Int. J. Mol. Sci.*, **11**: 3459-3471 (2010).